Direct regularization from co-registered contrast MRI improves image quality of MRI-guided near-infrared spectral tomography of breast lesions

Limin Zhang,

Thayer School of Engineering, Dartmouth College, Hanover NH 03755, College of Precision Instrument and Optoelectronics Key Engineering, Tianjin University, Tianjin 300072, China, and also with Tianjin Laboratory of Biomedical Detecting Techniques and Instrument, Tianjin 300072, China

Shudong Jiang,

Thayer School of Engineering, Dartmouth College, Hanover NH 03755

Yan Zhao,

Thayer School of Engineering, Dartmouth College, Hanover NH 03755

Jinchao Feng [Member, IEEE],

Thayer School of Engineering, Dartmouth College, Hanover NH 03755 and also with College of Electronic Information and Control Engineering, Beijing University of Technology, Beijing 100124, China

Brian W. Pogue, and

Thayer School of Engineering, Dartmouth College, Hanover NH 03755

Keith D. Paulsen [Member, IEEE]

Thayer School of Engineering, Dartmouth College, Hanover NH 03755

Abstract

An approach using direct regularization from co-registered DCE-MR images (DRI) was used to reconstruct Near-Infrared Spectral Tomography (NIRST) patient images, which does not need image segmentation. Twenty patients with mammography/ultrasound confirmed breast abnormalities were involved in this study, and the resulting images indicated that tumor HbT contrast differentiated malignant from benign cases (p-value=0.021). The approach produced reconstructed images which significantly reduced surface artifacts near the source-detector locations (p-value=4.16e-6).

Index Terms

Optical Imaging; Breast; Magnetic resonance Imaging; Image reconstruction

---

Correspondence to: Keith D. Paulsen.

I. Introduction

Breast cancer is the most common cancer among women in the US with an estimated of 252,710 new cases in 2017 [1]. Based on clinical research, odds of long-term survival are increased by early detection and treatment prior to tumor metastasis [2].

Current and emerging breast imaging techniques include X-ray mammography, Tomosynthesis, breast CT, ultrasound, and Magnetic Resonance Imaging (MRI), among others. X-ray mammography/Tomosynthesis are the current standard of care for breast cancer screening, and full-field digital mammography has an overall sensitivity and specificity reported to be 77% and 97% in a randomized multi-center trial [3]. However, mammography is much less effective in women with radiographically dense breasts [4], and cumulative radiation exposure limits its screening recommendations for younger women. Breast CT provides three-dimensional data by capturing multiple views of the breast at different angles, and offers new possibilities for detecting breast cancers. However, the radiation dose and false positive rates have limited its application as a clinical breast cancer screening tool to date. As a non-ionizing radiation modality, ultrasound is commonly used alongside mammography because of its differing contrast mechanisms, which makes it possible to detect lesions missed by x-ray imaging. A study found that when ultrasound was combined with X-ray mammography for screening dense breasts, ROC analysis yielded an Area Under the Curve (AUC) of 0.9 compared with 0.78 for mammography alone [5]. Though the combination of ultrasound and mammography has generated high sensitivity, the latter is not as high as it is for a contrast MRI exam [6].

Dynamic contrast enhanced magnetic resonance imaging (DCE-MRI) offers the highest sensitivity for breast lesion detection [5], and has experienced widespread implementation and rapid growth over the past 15 years [8]. Yet, universal adoption has been tempered by moderate specificity, which leads to excessive biopsies and related uncertainty about the value of the technique [9]. MRI is sensitive to changes in blood flow and blood volume as well as variations in blood oxygenation, but quantitative relationships between MRI signal and blood oxygenation are still unclear. Uncertainty in the value of MRI also exists in the setting of imaging treatment responses, where the signals are not as directly interpreted [10]–[12]. Still, methods to improve the specificity of breast DCE-MRI are of high interest given its exquisite sensitivity, and approaches which improve its specificity would be important, especially if they also improve the molecular and structural sensitivity of the technique, such as near-infrared spectral tomography (NIRST). While NIRST has potential, it suffers from low spatial resolution due to diffuse signal propagation in tissue, which is similar to other molecular sensing methods. Recently, we introduced a new approach for reconstructing NIRST data from DCE-MRI [13] which inputs images as templates for matrix regularization. In this paper, the new direct regularization from images (DRI) method is evaluated with clinical data to investigate its impact on the specificity of the MRI data.

Many molecular sensing methods suffer from spatial resolution limitations because of lack of signal strength, and the choice is often made to amplify the signal by averaging larger voxels as in MR spectroscopy [14], [15], diffusion MR [15], [16], positron emission tomography [17], [18]. However, the spatial limitation in NIRST arises from the diffuse

nature of the signal propagation which makes the inverse image reconstruction problem ill-posed mathematically [19]–[21]. Many methods to compensate for the ill-posed matrix inversion problem have been described, but most have invoked some assumptions about the tissue and how it can be segmented [22]–[29]. In the method studied here, DCE-MRI, itself, is used as the template for a regularization pattern of matrix voxels [13], [30], which incorporates an exponential weighting function based on voxel intensity. The application of this regularization approach has been studied in numerical simulations and a patient example [13], which showed that it offers two major benefits – suppression of surface artifacts and improved contrast in interior regions. These benefits compensate for two well-known concerns in NIRST, which limit its potential value. In this study, the methodology was applied to a data set of 20 subjects from a previously completed clinical trial. Methods to optimize the NIRST reconstruction accuracy from this data have yielded minor improvements in specificity [31], and the resulting NIRST images are still confounded by surface artifacts and low contrast recovery. The new method described here has potential to produce more accurate images with higher molecular specificity, and thereby to add diagnostic value to the DCE-MRI scans.

Equally important as the results is the concept that this new approach could be applied to a number of hybrid imaging modalities where one influences the recovered image accuracy of the other. Introduction of DRI regularization is a novel approach to combining images where values from one image guide recovery of the other image without requiring human intervention or manual segmentation.

II. Methods

A. Human Subject Imaging

The imaging protocol for human subject examination was approved by the Committee for the protection of human subjects at Dartmouth College and at Xijing Hospital in Xi'an, China. The study was carried out at Xijing Hospital in Xi'an, China. All patients received an explanation about the imaging process and signed a consent form before the imaging session was started. A total of 20 patients were involved in the study. Subsequent surgical pathology analysis confirmed 13 cases were malignant and 7 were benign.

B. Imaging System and Instrumentation

Patient data was collected using an MRI coupled NIRST system [32]. In this study, we prioritized the ease in which our optical interface was adapted to fit into commercially available breast MRI coils. Thus, in the present setting, MRI coupled NIRST has some of the same tissue coverage limitations as breast MRI. Fig. 1. provides an overview of the imaging system. Briefly, the subject was placed in prone position on a commercial MR breast coil (Fig. 1. top right). The breast with the abnormality was placed in a specially designed adjustable triangular interface which was attached within the open area of the coil (Fig. 1. bottom right). Six intensity-modulated (at 100MHz) and three continuous wavelength (CW) laser diodes, operating in the 660–950nm wavelength range, were used to generate light for signal transmissions. A set of 15 photo-multiplier tube (PMT) detectors (H9305-3, Hamamatsu) acquired both amplitude and phase data at wavelengths below

850nm, and a set of 15 silicon photodiode (PD) detectors (C10439-03, Hamamatsu) recorded only amplitude data in the longer wavelength range (900–950nm, Fig. 1. left). These data were used to estimate concentrations of oxy-hemoglobin (HbO_2), deoxy-hemoglobin (Hb), water, lipid and scattering properties (i.e., scattering power and scattering amplitude) in the breast. The triangular patient interface was designed to place 16 optical fiber bundles on the breast uniformly. Each time the source light was delivered to the breast through one of the fiber bundles, the diffused light resulting from the tissue was measured in parallel by the 15 PMT/PD detectors, coupled through the other 15 fiber bundles. MRI fiducial markers were placed at the ends of the fiber bundles for co-registration between MRI and optical images. MRI scans and optical measurements were performed simultaneously without interference between the two imaging modalities. Imaging time for a complete MRI and optical scan was about 30 mins and 15 mins, respectively.

C. Image Reconstruction and Analysis

Breast images were processed and reconstructed using NIR-FAST [33], an open source platform developed at Dartmouth. A direct regularization from co-registered DCE-MRI was used to reconstruct NIRST data [13]. In this image reconstruction approach, anatomical information from DCE-MRI was implemented directly in the inversion matrix regularization by encoding gray-scale image data into NIRST through a method termed Direct Regularization from Images (DRI). As described in detail in the previous paper [13], instead of setting the regularization matrix (L) to be an identity matrix as in the standard "no prior" reconstruction, DRI defines L as

$$L_{ij} = \begin{cases} 1 & i = j \\ -\dfrac{1}{M_i}\exp\left(-\dfrac{|\gamma_i - \gamma_j|^2}{2\sigma_g}\right), & otherwise \end{cases} \quad (1)$$

where γ_i is the anatomical image grayscale value in MRI mapped to position i in the NIRST image (grayscale values were normalized to the maximum within the image), σ_g is the characteristic grayscale difference over which to apply regularization, and M_i is a normalization factor chosen for each row.

Based on previous work [13], the regularization parameters λ and σ_g should be carefully selected to attain proper balance between stability and accuracy of the optical image reconstruction. Here, the initially fixed parameters $\lambda = 1$ and $\lambda = 10$, $\sigma_g = 0.001$ are used for no-priors and DRI methods, respectively.

Tumor region of interest (ROI) was defined for each patient by the reading radiologists according to the subject's DCE-MRI exam. For quantitative comparison of DRI and no-prior methods, tumor HbT contrast, which is the ratio of the average HbT inside to outside of the ROI was calculated.

A common problem with reconstructed NIRST images is the appearance of surface artifacts near the optical sources and detectors. To compare quantitatively the surface artifacts

generated by "no-prior" and DRI approaches, nodes per area within a distance of 15 mm from each fiber bundles were evaluated and the Standard Error (=Standard deviation/mean) of HbT was calculated as a performance measure.

D. Statistical Analysis

Patient results were analyzed by comparing malignant (n = 13) and benign (n = 7) groups, and a student's t-test was utilized to evaluate the performance of the DRI method. A two-tailed distribution was considered with significance achieved at the 95% confidence interval. Receiver-operating characteristic (ROC) curve analysis was carried out and the Area-Under-the-Curve (AUC) was examined as a way to quantify test performance [34], [35].

III. Results

Figure 2 shows the DCE-MRI and NIRST HbT (total hemoglobin concentration) images of a 46 year old patient with cancer. Axial, coronal and sagittal DCE-MRI (Fig. 2(a)) presented a $11 \times 16 \times 14$ mm lump in the top central portion (11:00 clock-face) of the right breast. The surgical pathology results from her mastectomy confirmed the lump was an invasive ductal carcinoma (IDC). Relative to HbT images reconstructed with no prior information, the DRI method significantly improved tumor to normal tissue contrast, as well as the localization of malignant lesion position and size. In addition, the artifacts in Fig. 2(b) have been significantly abated by encoding DCE-MRI structure into NIRST image reconstruction (Fig. 2 (c)).

Similar improvement occurred in a patient with a benign abnormality. Figure 3 illustrates the DCE-MRI and HbT images of 23-year-old patient with a regionally distributed benign lesion (adenosis) in the right half of the left breast. Artifacts appear (hot spot in the axial view) in HbT images reconstructed with no priors (Fig. 3(b)) that are suppressed with the DRI method (Fig. 3 (c)). Compared to the malignant case shown in Fig. 2, contrast in this benign lesion was reduced by the DRI method relative to the no-priors approach.

For a quantitative comparison of the surface artifacts in the images reconstructed by the "no-prior" and DRI methods, boxplots of standard errors are shown in Figure 4. DRI reconstruction yielded a significant reduction in surface artifacts (P-value $\ll 0.001$).

Table 1 lists the HbT tumor to normal tissue contrast for each patient, obtained by DRI and "no prior" methods, respectively. Correspondingly, the means and standard deviations for the malignant and benign groups are summarized in Table 2.

Boxplots of tumor HbT contrast for the two groups are illustrated in Figure 5. In Table 2 and Figure 5, mean HbT contrast was significantly higher in malignant relative to benign cases. Figure 5 shows that compared with the "no-prior" method HbT contrast obtained by DRI for malignant cancers had considerably more variation. The ratio of mean malignant contrast to mean benign contrast was $2.25\times$ and $1.54\times$ for DRI vs. "no prior" methods. The P-values, AUC, sensitivity and specificity obtained by DRI, No priors and DCE are listed in Table III. While the "no-prior" reconstructed HbT contrast provided border-line significance (p-value = 0.05), the P-value of DRI was 0.02, indicating that tumor HbT contrast can differentiate

malignant from the benign lesions. The AUC value is 0.77 using DRI only. When DCE-MRI and DCE-guided NIRST(DRI) are combined for diagnosis, the AUC increased from 0.82 to 0.9. Although the specificity obtained by DRI was optimal (1.00), it was dominated by the DCE value of 0.71, when the DRI and DCE-MRI data were combined and the statistical analysis returned a cutoff value that maximized the sum of sensitivity and specificity. Alternately, when maximizing specificity alone, the combined DRI and DCE-MRI data achieved a value of 1.00, but sensitivity suffered significantly (as shown in parentheses in Table III). No particularly attractive compromise between sensitivity and specificity was available in the combined DRI and DCE-MRI data, likely because of the relatively small sample size used in the study.

Further, figure 6 shows images of HbO_2 and Hb for the case studies shown in Fig. 2 and Fig. 3. Tumors are localized in Hband HbO_2 as well. P-values of 0.03 and 0.33 for Hb and HbO_2 resulted from comparisons of means between the benign and malignant groups, indicating that only Hb had statistical significance in differentiating malignant from benign cases in the small group of patients enrolled in the study.

IV. DISCUSSION

Results from 20 patient cases indicate that tumor contrast estimated from the images reconstructed by the DRI method can distinguish malignant from benign lesions. To date, optical image recovery in MRI-guided NIRST has been based on procedures that require segmentation, which is time consuming for users and requires radiological or anatomical training. Although the significance levels used to distinguish malignant from benign lesions examined here were lower than those for the previous segmentation-based methods, the DRI method is a fully automated image reconstruction process.

Without using DCE-MRI information, tumor HbT contrast obtained by the "no-prior" method was marginally significant in distinguishing malignant from benign lesions. Additionally, as shown in Fig 2(b) and Fig 3 (b), surface artifacts are significant, and affect the accuracy of identifying tumor size and location. In some cases, artifacts appeared in the abnormal ROI and resulted in HbT values being incorrect. By directly encoding structural information from DCE-MRI, the DRI method effectively suppressed artifacts so that image quality was improved. As discussed in our previous paper [13], image reconstruction artifacts are suppressed with the DRI approach (more than without it) because the structural prior information incorporated from DCE-MRI encodes spatial shapes in the image updates, which mimic the (MRI) gray scale intensity map. A Tikhonov framework is used as the regularization method

$$S(x) = \|f(x) - d\|_2^2 + \lambda\|Lx\|_2^2 \quad (2)$$

where L is the regularization matrix. The first term, defined as model error, represents the deviation of the observed image from the model observation. The second term, defined as the prior error, is the deviation of the image estimate from prior knowledge. L is an identity matrix in a no prior case, whereas in the DRI case, L is a weighting function based on the

anatomical (MRI) image grayscale map. Since the reconstructed image is constrained by structural priors through the regularization matrix, artifacts can be suppressed in DRI cases relative to a no-prior image reconstruction. However, the artifacts that do or do not appear arise from a combination of the gray scale patterns in the MRI data, as well as noise in the measured optical signals. Predicting the dominant effect (artifact suppression through spatial priors versus artifact amplification through optical measurement noise) is difficult; however, our results suggest that when the lower gray scale values from a benign case are included, the overall number of artifacts which appear in the image is reduced.

From HbT images obtained by the DRI method, (Fig. 2(c) and Fig. 3(c)), tumor size was smaller than the size estimated from DCE-MRI. The reduction in tumor size is likely due to limitations in mesh size used to keep computation time in a moderate range. This limitation caused loss of DCE-MRI information in some pixels in the regularization matrix. In addition, the loss of MRI information resulted in less or no improvement in some cases, relative to the "no-prior" method.

In Table 1, seven cases resulted in HbT contrast values below 1 with the DRI method was used. From a physiological point of the view, HbT tumor contrast is anticipated to be greater than unity because of increased tumor vascularization relative to the surrounding normal tissue. Because of the small number of patients considered here and the limited pathology data that were available from these subjects, a cause for the low HbT tumor contrast in some cases cannot be identified. One possible explanation would be that the tumor location is not perfectly well-demarcated by DCE-MRI in these cases, and as a result, is not recovered accurately by NIRST image reconstruction which is weighted by the MRI image gray scale.

The HbT contrasts of patients 8, 4 and18 are lower in the DRI relative to that in "no prior". The possible reason may due to the fact that the DRI method relies on the tumor grey scale contrast in DCE-MRI. Although the contrast values in a small portion of the patient cases are lower than that of "no prior", the overall p-values of HbT contrasts obtained by DRI has been obviously improved as compared to than that of "no prior" case, since DRI reduced the artifacts appearing in the images.

In addition to the clinical data obtained from DCE-MRI, HbT as well as other parameters (i.e., blood oxygenation, water and lipid) acquired with NIRST provides information on tissue function beyond contrast was-in/wash-out kinetics.

V. Conclusion

Results presented in this paper demonstrate the feasibility and robustness of a hybrid MRI-NIRST approach for breast imaging. The fully-automated DRI method increased tumor contrast in HbT, improved the accuracy of tumor position and size, and decreased the presence of surface artifact relative to using "no prior" in diffuse tomography. Importantly, HbT contrast showed a significant difference between malignant lesions and benign conditions. The result is a step towards non-invasive assessment of benign/malignant tumors.
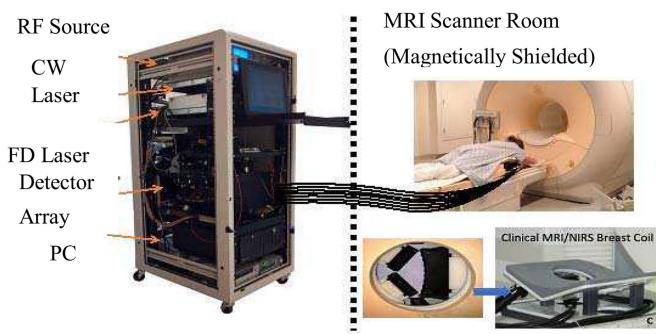
Acknowledgments

References

1. American Cancer Society. Cancer Facts and Figures 2017. 2017

2. Tabar L, Yen MF, Vitak B, Chen HH, Smith RA, Duffy SW. Mammography service screening and mortality in breast cancer patients: 20-year follow-up before and after introduction of screening. Lancet. 2003; 361:1405–1410. [PubMed: 12727392]

3. Skaane P, Hofvind S, Skjennald A. Randomized trial of screen-film versus full-field digital mammography with soft-copy reading in population-based screening program: follow-up and final results of Oslo II study. Radiology. 2007; 244:708–717. [PubMed: 17709826]

4. Carney PA, Miglioretti DL, Yankaskas BC, Kerlikowske K, Rosenberg R, Rutter CM, Geller BM, Abraham LA, Taplin SH, Dignan M, Cutter G, Barbash RB. Individual and combined effects of age, breast density, and hormone replacement therapy use on the accuracy of screening mammography. Ann Intern Med. 2003; 138:168–175. [PubMed: 12558355]

5. Berg WA, Blume JD, Cormack JB, Mendelson EB, Lehrer D. Combined Screening With Ultrasound and Mammography vs Mammography Alone in Women With Elevated Risk of Breast Cancer. JAMA-J Am Med Assoc. 2008; 299:2151–2163.

6. Berg WA, Gutierrez L, NessAiver MS, Carter WB, Bhargavan M, Lewis RS, Ioffe OB. Diagnostic Accuracy of Mammography, Clinical Examination, US, and MR Imaging in Preoperative Assessment of Breast Cancer1. Radiology. 2004; 233:830–949. [PubMed: 15486214]

7. Bluemke DA, Gatsonis CA, Chen MH, DeAngelis GA, DeBruhl N, Harms S, Heywang-Kobrunner SH, Hylton N, Kuhl CK, Lehman C, et al. Magnetic resonance imaging of the breast prior to biopsy. JAMA. 2004; 292:2735–2742. [PubMed: 15585733]

8. Stout NK, Nekhlyudov L, Li L, Malin ES, Ross-Degnan D, Buist DS, Rosenberg MA, Alfisher MSW, Fletcher. Rapid increase in breast magnetic resonance imaging use: trends from 2000 to 2011. JAMA. Intern. Med. 2014; 174:114–121. [PubMed: 24247482]

9. Wernli KJ, DeMartini WB, Ichikawa L, Lehman CD, Onega T, Kerlikowske K, Henderson LM, Geller BM, Hofmann M, Yankaskas BC. Patterns of breast magnetic resonance imaging use in community practice. JAMA. Intern. Med. 2014; 174:125–132. [PubMed: 24247555]

10. Lee JM, Orel SG, Czerniecki BJ, Solin LJ, Schnall MD. MRI before reexcision surgery in patients with breast cancer. AJR. Am. J. Roentgenol. 2004; 182:473–480. [PubMed: 14736685]

11. Kuzucan A, Chen JH, Bahri S, Mehta RS, Carpenter PM, Fwu PT, Yu HJ, Hsiang DJ, Lane KT, Butler JA, et al. Diagnostic performance of magnetic resonance imaging for assessing tumor response in patients with HER2-negative breast cancer receiving neoadjuvant chemotherapy is associated with molecular biomarker profile. Clin. Breast Cancer. 2012; 12:110–118. [PubMed: 22444717]

12. Quinn EM, Coveney AP, Redmond HP. Use of magnetic resonance imaging in detection of breast cancer recurrence: a systematic review. Ann. Surg. Oncol. 2012; 19:3035–3041. [PubMed: 22476755]

13. Zhang L, Zhao Y, Jiang S, Pogue BW, Paulsen KD. Direct regularization from co-registered anatomical images for MRI-guided near-infrared spectral tomographic image reconstruction. Biomed. Opt. Exp. 2015; 6:13.

14. Schmitz AM, Veldhuis WB, Menke-Pluijmers MB, van der Kemp WJ, van der Velden TA, Kock MC, Westenend PJ, Klomp DW, Gilhuijs KG. Multiparametric MRI With Dynamic Contrast Enhancement, Diffusion-Weighted Imaging, and 31-Phosphorus Spectroscopy at 7T for Characterization of Breast Cancer. Invest. Radiol. 2015; 50:766–771. [PubMed: 26135017]

15. Sharma U, Sah RG, Parshad R, Sharma R, Seenu V, Jagannathan NR. Role of apparent diffusion coefficient values for the differentiation of viable and necrotic areas of breast cancer and its potential utility to guide voxel positioning for MRS in the absence of dynamic contrast-enhanced MRI data. Magn. Reson. Imaging. 2012; 30:649–655. [PubMed: 22459442]

16. Partridge SC, Singer L, Sun R, Wilmes LJ, Klifa CS, Lehman CD, Hylton NM. Diffusion-weighted MRI: influence of intravoxel fat signal and breast density on breast tumor conspicuity and apparent diffusion coefficient measurements. Magn. Reson. Imaging. 2011; 29:1215–1221. [PubMed: 21920686]

17. Atuegwu NC, Li X, Arlinghaus LR, Abramson RG, Williams JM, Chakravarthy AB, Abramson VG, Yankeelov TE. Longitudinal, intermodality registration of quantitative breast PET and MRI data acquired before and during neoadjuvant chemotherapy: preliminary results. Med. Phys. 2014; 41:052302. [PubMed: 24784395]

18. Dmitriev ID, Loo CE, Vogel WV, Pengel KE, Gilhuijs KG. Fully automated deformable registration of breast DCE-MRI and PET/CT. Phys. Med. Biol. 2013; 58:1221–1233. [PubMed: 23369926]

19. Dehghani H, Pogue BW, Jiang S, Brooksby B, Paulsen KD. Three-dimensional optical tomography: resolution in small-object imaging. Appl. Opt. 2003; 42:3117–3128. [PubMed: 12790463]

20. Pogue BW, Davis SC, Song X, Brooksby BA, Dehghani H, Paulsen KD. Image analysis methods for diffuse optical tomography. J. Biomed. Opt. 2006; 11:33001. [PubMed: 16822050]

21. Pogue BW, Davis SC, Leblond F, Mastanduno MA, Dehghani H, Paulsen KD. Implicit and explicit prior information in near-infrared spectral imaging: accuracy, quantification and diagnostic value. Philos. Transact. A. Math Phys. Eng. Sci. 2011; 369:4531–4557.

22. Ntziachristos V, Yodh AG, Schnall M, Chance B. Concurrent MRI and diffuse optical tomography of breast after indocyanine green enhancement. Proc. Natl. Acad. Sci. USA. 2000; 97:2767–2772. [PubMed: 10706610]

23. Ntziachristos V, Yodh AG, Schnall MD, Chance B. MRI-guided diffuse optical spectroscopy of malignant and benign breast lesions. Neoplasia. 2002; 4:347–354. [PubMed: 12082551]

24. Brooksby B, Srinivasan S, Jiang S, Dehghani H, Pogue BW, Paulsen KD, Weaver J, Kogel C, Poplack SP. Spectral priors improve near-infrared diffuse tomography more than spatial priors. Opt. Lett. 2005; 30:1968–1970. [PubMed: 16092235]

25. Brooksby B, Pogue BW, Jiang S, Dehghani H, Srinivasan S, Kogel C, Tosteson TD, Weaver J, Poplack SP, Paulsen KD. Imaging breast adipose and fibroglandular tissue molecular signatures by using hybrid MRI-guided near-infrared spectral tomography. Proc. Natl. Acad. Sci. USA. 2006; 103:8828–8833. [PubMed: 16731633]

26. Carpenter CM, Srinivasan S, Pogue BW, Paulsen KD. Methodology development for three-dimensional MR-guided near infrared spectroscopy of breast tumors. Opt. Express. 2008; 16:17903–17914. [PubMed: 18958072]

27. Carpenter CM, Rakow-Penner R, Jiang S, Pogue BW, Glover GH, Paulsen KD. Monitoring of hemodynamic changes induced in the healthy breast through inspired gas stimuli with MR-guided diffuse optical imaging. Med. Phys. 2010; 37:1638–1646. [PubMed: 20443485]

28. Choe R, Corlu A, Lee K, Durduran T, Konecky SD, Grosicka-Koptyra M, Arridge SR, Czerniecki BJ, Fraker DL, DeMichele A, et al. Diffuse optical tomography of breast cancer during neoadjuvant chemotherapy: a case study with comparison to MRI. Med. Phys. 2005; 32:1128–1139. [PubMed: 15895597]

29. Mastanduno MA, Xu J, El-Ghussein F, Jiang S, Yin H, Zhao Y, Wang K, Ren F, Gui G, Pogue BW, Paulsen KD. MR-Guided Near-Infrared Spectral Tomography Increases Diagnostic Performance of Breast MRI. Clin. Cancer. Res. 2015; 21:3906–3912. [PubMed: 26019171]

30. Holt RW, Davis S, Pogue BW. Regularization functional semi-automated incorporation of anatomical prior information in image-guided fluorescence tomography. Opt. Lett. 2013; 38:2407–2409. [PubMed: 23939063]

31. Zhao Y, Mastanduno MA, Jiang S, Ei-Ghussein F, Gui J, Pogue BW, Paulsen KD. Optimization of image reconstruction for magnetic resonance imaging-guided near-infrared diffuse optical spectroscopy in breast. J. Biomed. Opt. 2015; 20:56009. [PubMed: 26000795]

32. El-Ghussein F, Mastanduno MA, Jiang S, Pogue BW, Paulsen KD. Hybrid photomultiplier tube and photodiode parallel detection array for wideband optical spectroscopy of the breast guided by magnetic resonance imaging. J. Biomed. Opt. 2014; 19:011010. [PubMed: 23979460]

33. Dehghani H, Eames ME, Yalavarthy PK, Davis SC, Srinivasan S, Carpenter CM, Pogue BW, Paulsen KD. Near infrared optical tomography using NIRFAST: Algorithm for numerical model and image reconstruction. Commun. Numer. Meth. En. 2009; 25:711–732.

34. Metz CE. Basic principles of ROC analysis. In Seminars in nuclear medicine. Elsevier. 1978:283–298.

35. Swets JA. Measuring the accuracy of diagnostic systems. Science. 1988; 240:1285–1293. [PubMed: 3287615]
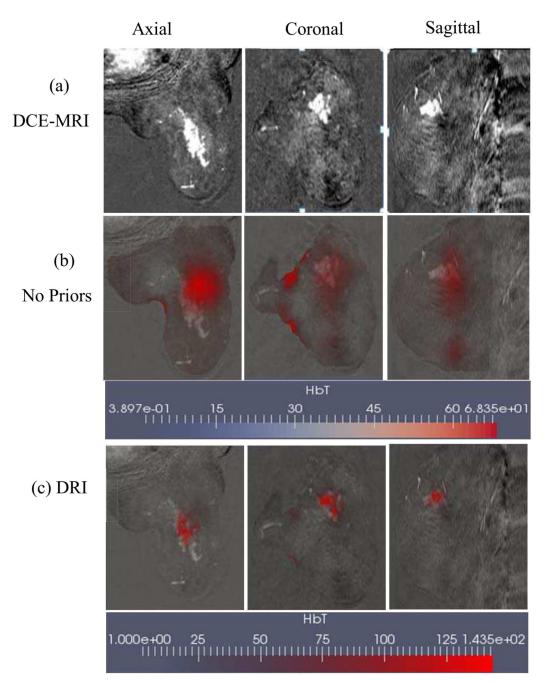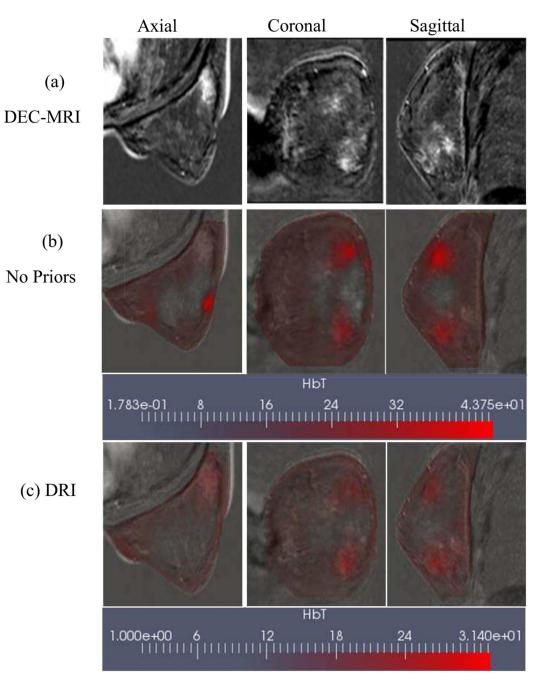
Fig. 1.
Overview of NIRST system. Six frequency domain laser diodes are driven by RF signal generators at 100MHz and three CW lasers are driven directly by computer generated currents. Light is delivered to the breast through 16 sequential source fibers. An array of 15 PMTs and 15 Photodetectors measure amplitude and phase of collected light. Optical fibers are housed within an MRI breast coil (right bottom) and the optical and MRI exam are conducted simultaneously.
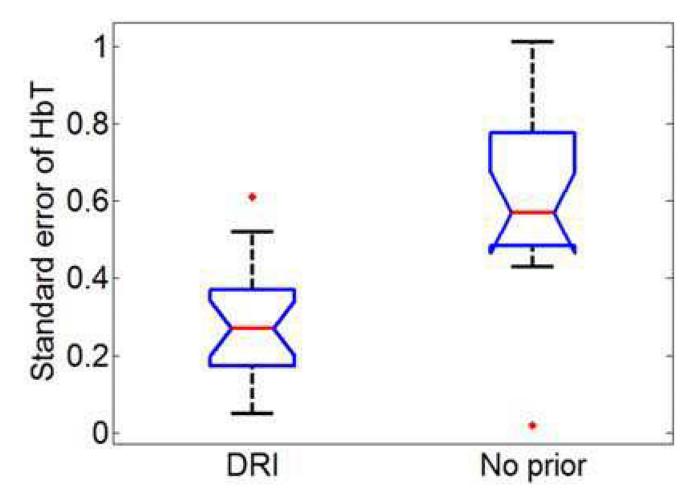
Fig. 2.
DCE-MRI and NIRST HbT images of a patient with a $11 \times 16 \times 14$ mm invasive ductal carcinoma (IDC) in the right breast. (a) DCE-MRI and optical images reconstructed by no-priors (b) and DRI (c). HbT images are overlaid on the DCE- MRI slices.
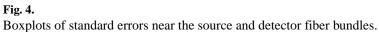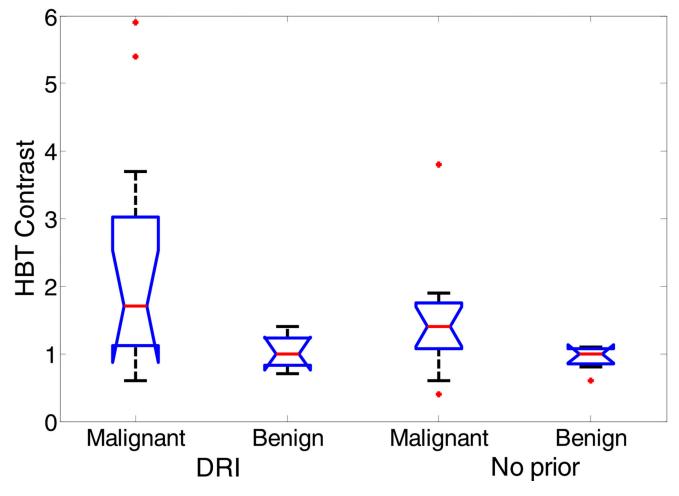
Fig. 3.
DCE-MRI and NIRST HbT images of a patient with adenosis (benign). (a) The DCE-MRI; and optical images reconstructed by nopriors (b) and DRI (c). The HbT images reconstructed with $\lambda = 1$ for no priors and DRI methods with $\lambda = 10$ and $\sigma_g = 0.001$, respectively.

Fig. 4.
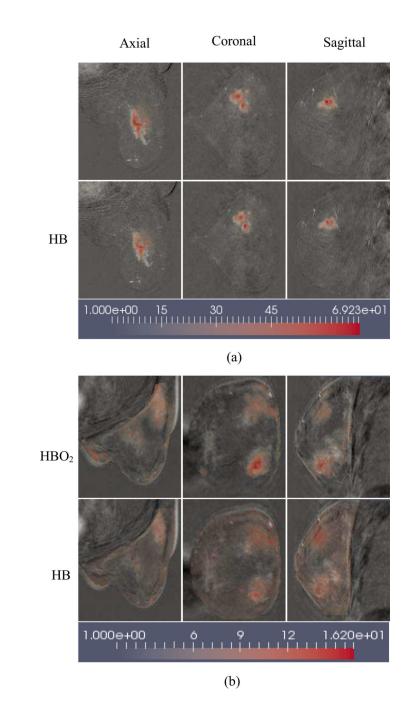Boxplots of standard errors near the source and detector fiber bundles.

Fig. 5.
Boxplots of HbT contrast in malignant (n = 13) and benign (n = 7) groups, obtained by DRI and "no prior" methods.

(a)

(b)

Fig. 6.
The oxy-hemoglobin (HBO2) and deoxy-hemoglobin (Hb) images of IDC (a) and benign (b) calculated by DRI method, corresponding to the patients in Fig. 2 and Fig. 3 respectively.

TABLE I

List of Tumor HbT Contrast for Each Patient, Obtained by DRI and No Prior Methods, Respectively

Pt #	Pathology	HBT Contrast	
		DRI method	**No priors**
1	IDC	1.24	1.23
2	IDC	0.67	0.57
3	IDC	0.64	0.36
4	IDC	5.36	1.75
5	IDC	3.72	1.59
6	IDC	1.80	1.04
7	IDC	1.43	1.10
8	DC	0.91	1.24
9	IDC	1.84	1.85
10	IDC	1.69	1.41
11	IDC	1.73	1.37
12	IDC	2.76	1.86
13	IDC	5.75	3.68
14	adenosis	0.68	0.83
15	Fibroadenoma	1.25	1.25
16	adenosis	1.17	1.01
17	Fibroadenoma	0.96	0.94
18	Fibroadenoma	0.76	1.00
19	Intraductal papilloma	1.45	1.07
20	Cystic hyperplasia	0.88	0.64

TABLE II

The Means and Standard Deviations of HbT Contrast for the Malignant and Benign

	DRI		No-prior	
	Malignant (n=13)	Benign (n=7)	Malignant (n=13)	Benign (n=7)
Mean	2.29	1.02	1.48	0.96
Standard Deviation	1.76	0.28	0.84	0.19

TABLE III

P-Values, AUC, Optimal Cutoff, Sensitivity and Specificity Obtained by DRI, No Priors and DCE-MRI

	DRI	No priors	DCE	DRI+DCE
P-values	0.02	0.05	0.005	0.012
AUC	0.77	0.79	0.82	0.90
Optimal cutoff	1.57	1.09	/	/
Sensitivity	0.60	0.77	0.92	1.00(0.62 [*])
Specificity	1.00	0.86	0.71	0.71(1.00 [*])

[*] Specificity and sensitivity when maximizing specificity alone.